

## Electro-optical characterization of SiPM: A comparative study

N. Dinu <sup>\*,1</sup>, Z. Amara, C. Bazin, V. Chaumat, C. Cheikali, G. Guilhem, V. Puill, C. Sylvia, J.F. Vagnucci

Laboratory of Linear Accelerator (LAL), IN2P3-CNRS, 91898 Orsay, France

### ARTICLE INFO

Available online 22 May 2009

#### Keywords:

Photodetectors  
Silicon PhotoMultiplier  
Gain  
Dark count rate  
Photon detection efficiency

### ABSTRACT

This work reports on the development of an electro-optical set-up for the characterization of the Silicon PhotoMultiplier (SiPM) devices as well as on the comparative study of the characteristics of different SiPM prototypes. The electrical set-up allows the measurement of the static (breakdown voltage, overvoltage quenching resistance) and dynamic (gain, dark count rate) characteristics. The optical set-up allows the estimation of the photon detection efficiency as a function of the wavelength and the operation voltage. The comparative study has been performed on SiPM devices covering an area of  $1 \times 1 \text{ mm}^2$  and supplied during 2007 by Photonique S.A. (Switzerland), FBK-irst (Italy), SensL (Ireland) and Hamamatsu (Japan).

© 2009 Elsevier B.V. All rights reserved.

### 1. Introduction

Nowadays, the Silicon PhotoMultiplier (SiPM) [1–3] has become an attractive alternative to the photomultiplier tubes and avalanche photodiodes (APD) for applications like high-energy physics (e.g. HCAL & ECAL detectors of the ILC), medical imaging (e.g. PET) or astrophysics (e.g. T2K). In order to match these requests, the manufacturers made fast progresses and they proposed various devices with different characteristics [4–7].

The choice of the SiPM device appropriate to each application is strongly dependent on its characteristics. Therefore, the development of a calibrated electro-optical set-up allowing the characterization of different SiPM devices in similar operational conditions as well as the comparative analysis of the SiPM characteristics represent an important task.

In this paper, a description of the main electro-optical characteristics of the SiPM devices will be given. In particular, (a) static characteristics as breakdown voltage, overvoltage, quenching resistance, (b) dynamic parameters as gain and dark count rate and (c) optical parameters as photon detection efficiency (PDE) will be presented. The dedicated set-ups developed in our laboratory for the measurement of the mentioned parameters will be described. Using these set-ups, the characteristics of the SiPM's covering an area of  $1 \times 1 \text{ mm}^2$  and supplied by Photonique, FBK-irst, SensL, Hamamatsu HPK during 2007 have been measured, leading to a comparative analysis reported also in this paper.

### 2. The SiPM parameters and dedicated electro-optical experimental set-ups

The SiPM consists of a matrix of hundreds of micro-cells ( $\mu\text{cell}$ ) connected in parallel on a common silicon substrate. Each  $\mu\text{cell}$  is represented by a Geiger-mode avalanche photodiode (GM-APD) connected in series with its integrated passive quenching resistance.

During the Geiger-mode operation, each GM-APD is biased to a voltage  $V_{\text{bias}}$  above the breakdown voltage  $V_{\text{BD}}$ . The  $V_{\text{bias}}$  exceeds the  $V_{\text{BD}}$  by an amount called overvoltage  $\Delta V = V_{\text{bias}} - V_{\text{BD}}$ , which has a determining influence on detector performance (e.g. the ratio  $\Delta V/V_{\text{BD}}$  is related to the excess electric field above the breakdown level). Consequently, the first parameters required to be evaluated for a SiPM device are  $V_{\text{BD}}$  and the  $\Delta V$ . These parameters can be determined from the reverse IV current-voltage characteristic.

If a primary carrier is generated in the sensitive area of a SiPM device by an incident photon or a thermal generated carrier, a very high current signal is produced. The continuous flow of the current in the external circuit is limited by the quenching resistance, which quenches the avalanche and allows lowering the  $V_{\text{bias}}$  to  $V_{\text{BD}}$  or below. The  $V_{\text{bias}}$  is then restored during a recovery time  $\tau_{\text{recovery}}$  depending on the values of the  $\mu\text{cell}$  quenching resistance and capacitance ( $\tau_{\text{recovery}} \sim 2.2 R_{\text{q}\mu\text{cell}} \times C_{\mu\text{cell}}$  to recover from 10% to 90%). Therefore, the value of the  $R_{\text{q}\mu\text{cell}}$  influences the time required for a  $\mu\text{cell}$  to recover its operation voltage and to be able to detect another incident photon and it represents another important parameter to be determined. It can be also evaluated from the forward IV characteristic.

For the measurement of the IV reverse and forward characteristics, a first electrical set-up has been build (DC set-up); it consists of the SiPM connection to a Keithley source-meter ( $I_{\text{resolution}} \sim 2 \text{ pA}$ ) through triaxial cables ( $R_{\text{isolation}} \sim 10 \text{ T}\Omega$ ).

\* Corresponding author. Tel.: +33 1 6446 8383; fax: +33 1 6446 8500.

E-mail address: [dinu@lal.in2p3.fr](mailto:dinu@lal.in2p3.fr) (N. Dinu).

<sup>1</sup> On leave from Institute of Space Sciences, Bucharest, Romania.

The dynamic parameters dominating the performances of a SiPM device in many applications are as follows: (1) the gain ( $G$ ), defined as the charge developed during one Geiger avalanche divided by the electron charge; and (2) the dark count rate (DCR), defined as the number of false photon counts per second registered in the absence of the light. For the measurement of these parameters, a second electrical set-up has been built (AC set-up); it allows the bias of the SiPM by the Keithley and its read-out by an MITEQ wide-band (0.01–500 MHz) voltage amplifier connected to a Tektronix digital oscilloscope (500 MHz, 5 GS/s). The amplifier presents  $50\Omega$  input impedance, which acts as a current-to-voltage converter followed by an amplifying stage having a gain of 45 dB.

LabView and C+ programs have been developed for the automatic data acquisition and analysis of the SiPM parameters mentioned above. A controlled temperature ( $25 \pm 0.5^\circ\text{C}$ ) of both static and dynamic electrical tests has been assured by an LMS Fisher Bioblock climatic chamber. Since the signals triggered by a thermal generated carrier or by an absorbed photon are identical, the mentioned parameters were tested in dark conditions and the only parameter tested in light conditions was the photon detection efficiency.

For a photon to be detected by a SiPM, it must be absorbed in the detector active area, it should generate a primary carrier (more precisely an electron–hole pair) and of course the primary carrier should succeed in triggering an avalanche. Therefore, the PDE of a SiPM depends on three parameters: the geometrical efficiency  $\varepsilon_{\text{geom}}$  (the ratio of the sensitive area on the total detector surface), the quantum efficiency QE (wavelength ( $\lambda$ ) dependent) and the triggering probability  $\varepsilon_{\text{trigger}}$  (linked to the impact ionization rates of electrons and holes).

Therefore, PDE analysis as a function of incident  $\lambda$  and  $\Delta V$  is very important and an optical set-up has been developed. It is composed of a halogen continuous light source (100 W) followed by a grating monochromator, which separates the visible wavelengths (350–800 nm) with an accuracy of 2 nm. The number of incident photons, evaluated by two calibrated PIN photodiodes (HPK S3590-18, UDT Instrument 221), is kept constant and low ( $\sim 10^7$ /incident photons/s/mm<sup>2</sup>) to avoid SiPM saturation. The precise replacement in front of the beam light in between the calibrated photodiodes and the SiPM was assured by Polytec PI xyz translation stage (6  $\mu\text{m}$  accuracy on each direction). The optical tests have been performed at controlled room temperature ( $25 \pm 1^\circ\text{C}$ ).

The number of photons detected by the SiPM has been evaluated by both the photocurrent and the photon counting techniques using the DC and the AC set-ups, respectively. More details on the PDE as well as the  $G$  and DCR calculation can be found in Ref. [8].

### 3. The characteristics of the SiPM prototypes

The geometrical characteristics of analyzed prototypes (indicated by the producers) are presented in Table 1. It can be noticed that, even if all devices cover an area of  $1 \times 1 \text{ mm}^2$ , the size of  $\mu\text{cells}$  (implicitly the number of  $\mu\text{cells}$ ) as well as the  $\varepsilon_{\text{geom}}$  is variable from one device to the other, depending on the producer design and technology.

The static characteristics (reverse and forward IV plots) of all SiPM prototypes are presented in Fig. 1(a) and (b). The IV plots are shown as a function of the Abs  $V_{\text{bias}}$  to simplify the graphical representation. In reality, based on the polarity of the  $V_{\text{bias}}$  applied in between the substrate and the front side of the SiPM, the type of silicon substrate used to build the device can be determined (e.g. for  $n^+$ /p  $\mu\text{cells}$  build on p-type substrate, a negative  $V_{\text{bias}}$  has

**Table 1**  
Geometrical characteristics of the SiPM prototypes.

Producer	SiPM ID	No. $\mu\text{cells}$	$\mu\text{cell}$ size ( $\mu\text{m}$ )	$\varepsilon_{\text{geom}}$ (%)
Photonique	SSPM-0701-BG	556	$43 \times 43$	70
FBK-irst	W20-B10-T3V2PD/I run	625	$40 \times 40$	20
FBK-irst	W3-B3-T6V1PD/II run	625	$40 \times 40$	16
SensL	SPM-20	848	$29 \times 32$	43
SensL	SPM-35	400	$44 \times 47$	59
SensL	SPM-50	216	$59 \times 62$	68
HPK	S10362-11-25	1600	$25 \times 25$	31
HPK	S10362-11-50	400	$50 \times 50$	61.6
HPK	S10362-11-100	100	$100 \times 100$	78.5

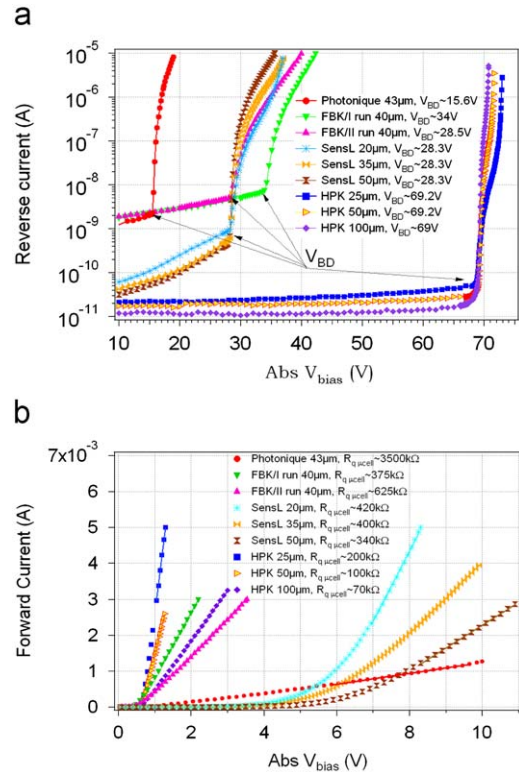


**Fig. 1.** (a) Reverse and (b) forward IV characteristics of the SiPM prototypes.

to be applied to the substrate with respect to the front side to obtain a reverse IV characteristic). Based on this experimental observation, a p-type substrate has been identified for the Photonique, FBK-irst and SensL devices, while the n-type substrate has been found for the HPK devices.

From Fig. 1(a), the  $V_{\text{BD}}$  values have been extracted (indicated in the legend). It can be noticed that a uniform  $V_{\text{BD}}$  has been measured over the devices coming from the same producer (e.g.  $V_{\text{BD SensL}} \sim 28.3 \text{ V}$ ,  $V_{\text{BD HPK}} \sim 69.2 \text{ V}$ ) independent of their geometrical characteristics, while different values ranging from 15 to 70 V have been measured over devices coming from different producers.

The dark current above  $V_{\text{BD}}$  represents the average current flowing through a  $\mu\text{cell}$  during 1 s and it depends on the  $G$  and the DCR. Assuming that a maximum value of  $\sim 10 \mu\text{A}$  can represent a good compromise in between the  $G$  and the DCR at a certain  $V_{\text{bias}}$  (will be confirmed by the AC measurements), the  $\Delta V/V_{\text{BD}}$  can be estimated. A  $\Delta V/V_{\text{BD}}$  ranging from 0% to 15% has been found for Photonique, FBK-irst and SensL devices, while  $\Delta V/V_{\text{BD}}$  ranging from 0 to 3–5% has been estimated for HPK devices.

From the linear fit of the forward IV plots, the values of  $R_{q\mu cell}$  can be calculated (indicated in the legend). It can be noticed that hundreds of  $k\Omega$  have been found for the  $R_{q\mu cell}$  of FBK-irst, SensL and HPK devices once much higher value of  $\sim$ thousands of  $k\Omega$  has been found for the Photonique device.

The dynamic analysis of different SiPM prototypes revealed a signal shape (indicating a Geiger avalanche) as shown in Fig. 2. Following these shapes, a  $\tau_{recovery}$  ranging from 10 ns up to 220 ns has been estimated for FBK-irst, SensL and HPK devices, once a much longer value ( $>300$  ns, not visible in the plot) has been estimated for Photonique device.

The  $G$  has been determined from the time integration of the output signals during an integration window to be equal to  $\tau_{recovery}$ . Fig. 3 confirms a linear variation of the  $G$  as a function of the  $\Delta V$  independent of the SiPM prototype, but with different slopes, as a function of the  $\mu cell$  geometry. The  $G$  ranges from  $1 \times 10^5$  to  $4 \times 10^6$ , once the  $C_{\mu cell}$ , calculated from the slope of the linear fits, shows values ranging from 25 to 500 fF for the FBK-irst, SensL and HPK devices. For what concerns the Photonique device, the  $G$  was calculated using an integration window of  $\sim 40$  ns, therefore much less than  $\tau_{recovery}$  corresponding to this device. This choice is correlated with  $G$  values reported in the data sheet provided by Photonique and it was determined by the experimental difficulties accounted for very long integration windows.

The DCR (counts/s) of different SiPM prototypes was studied as a function of the ratio  $\Delta V/V_{BD}$  (Fig. 4). Two remarks can be highlighted: (1) the Photonique, FBK-irst and SensL devices ( $n^+/p$   $\mu cells$  on p-type substrate) present a relatively slow parabolic increase of the DCR for  $\Delta V/V_{BD}$  up to 10–15%, once the HPK devices ( $p^+/n$   $\mu cells$  on n-type substrate) show a faster parabolic dependence for  $\Delta V/V_{BD}$  up to only few %; (2) the DCR of

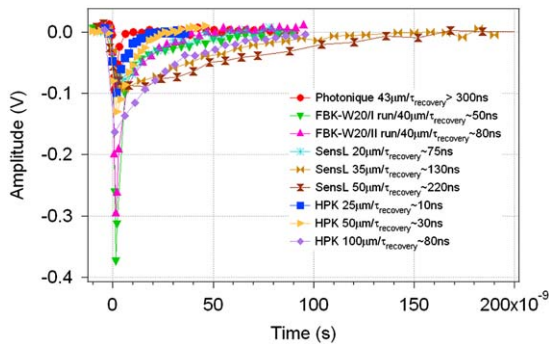


Fig. 2. Single- $\mu cell$  dark signals shape of the SiPM.

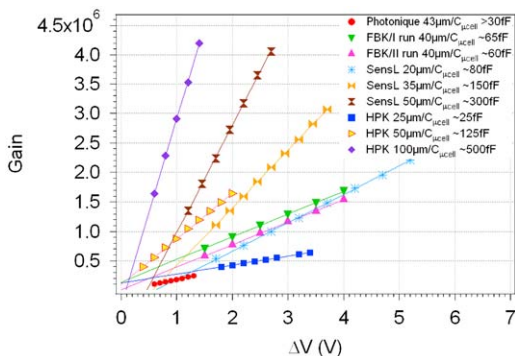


Fig. 3. The gain of the SiPM prototypes vs.  $\Delta V$ .

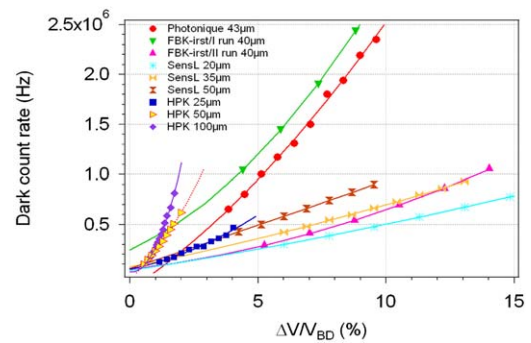


Fig. 4. The DCR of the SiPM prototypes vs.  $\Delta V/V_{BD}$ .

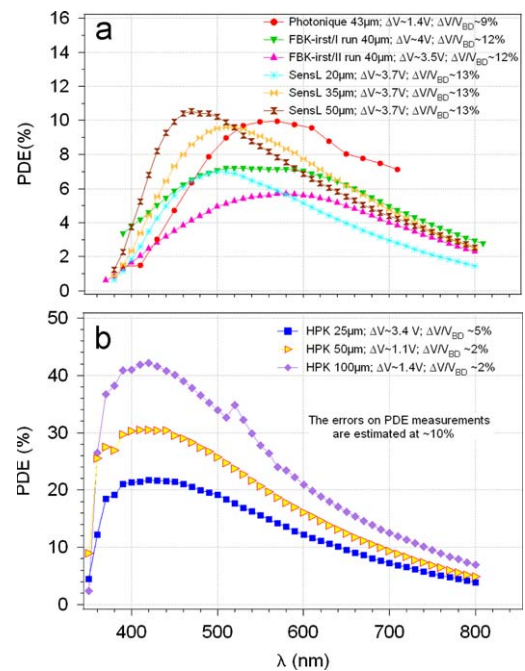


Fig. 5. (a) The PDE vs.  $\lambda$  of the Photonique, FBK-irst and SensL devices and (b) HPK devices.

Photonique and FBK-irst/I run devices ranges from 0.5 to 2.5 MHz for  $\Delta V/V_{BD}$  of 5–10%, the FBK-irst/II run and SensL devices present less than 1 MHz for  $\Delta V/V_{BD}$  up to 15% and HPK devices show less than 1 MHz for  $\Delta V/V_{BD}$  of few %.

As it has been noticed from the graphical representation of the DCR vs.  $\Delta V/V_{BD}$ , an optimal  $\Delta V/V_{BD}$  can be estimated for each device:  $\sim 10$ –13% for Photonique, FBK-irst and SensL devices and  $\sim 2$ –5% for HPK devices. If  $\Delta V/V_{BD}$  exceeds the indicated values, the DCR becomes too big and experimental difficulties can be found in applications where no external trigger can be used to announce the photons arrival.

An experimental set-up providing triggered light for the entire visible range is extremely difficult to build. Therefore, the PDE vs.  $\lambda$  ranging from 350 to 800 nm has been studied with continuous light, applying the optimal  $\Delta V/V_{BD}$  indicated above. The Photonique, FBK-irst and SensL devices (Fig. 5(a)) show maximum PDE values of  $\sim 6$ –10% in the green region (500–600 nm), while HPK devices (Fig. 5(b)) present maximum PDE values of  $\sim 20$ –40% in the blue region (420 nm). The main differences in between the PDE values could be explained by (1) a higher  $\epsilon_{trigger}$  corresponding to HPK devices ( $p^+/n$   $\mu cells$  on n-type substrate) with respect to the Photonique, FBK-irst and SensL devices ( $n^+/p$   $\mu cells$  on p-type substrate) for blue incident light and (2)

differences in between the  $\varepsilon_{\text{geom}}$  of different devices. A detail is required to be mentioned: the analyzed prototypes represent devices of very early production runs of different producers and some parameters are not yet optimized (e.g. the  $\varepsilon_{\text{geom}}$  of FBK-irst devices).

The development of a new set-up providing triggered light is in progress and a more exhaustive analysis of the PDE will be reported in a future article.

#### 4. Conclusions

In this paper, we reported on the development of an electro-optical set-up allowing the characterization of different SiPM devices in similar operational conditions. Using this set-up, the main SiPM parameters can be measured: the static, the dynamic as well as the optical ones. The set-up has been validated performing a comparative analysis of different SiPM supplied by Photonique, FBK-irst, SensL and HPK. All prototypes are fully

functional and the analyzed parameters show trends compatible with the operation principle of the device.

#### Acknowledgements

The authors would like to thank Dr. Adam Para for his help on the development of the LabView program allowing the data acquisition and SiPM characteristics analysis.

#### References

- [1] V.M. Golovin, et al., Russian Patent No. 1644708, 1999.
- [2] Z. Sadygov, Russian Patent No. 2086047 C1, 1997.
- [3] P. Buzhan, B. Dolgoshein, et al., ICFA Instrumentation Bulletin 23 (2001) 28.
- [4] <[http://www.photonique.ch/Prod\\_0701BG.html](http://www.photonique.ch/Prod_0701BG.html)>.
- [5] <<http://www.sensl.com>>.
- [6] <<http://www.hamamatsu.com>>.
- [7] C. Piemonte, et al., IEEE Transactions on Nuclear Science NS-54 (1, Part 2) (2007) 236.
- [8] N. Dinu, et al., these proceedings, doi:10.1016/j.nima.2009.05.080.